Progress In Electromagnetics Research C, Vol. 114, 233–246, 2021

On the Role of Time-Frequency Analysis for Joint DOD-DOA Estimation for Bistatic MIMO Radars

Yashvanth Lakshminarasimhan, Roshaan Soundarapandian, and Palanisamy Ponnusamy*

Abstract—RAdio Detection And Ranging (RADAR) is an essential tool used extensively to detect a target's presence within the vicinity characterized by the range of the RADAR. In order to localize the target, Direction of Departure (DOD) and Direction of Arrival (DOA) estimations are utilized. To make it more convenient, a bistatic multiple input multiple output (MIMO) configuration is exploited to deduce the position of a target through the triangulation method easily. Furthermore, due to the maneuvering of targets in space, more robust direction finding solutions can be derived using time-frequency (TF) representations. Thus, this paper aims to leverage the benefits of TF analysis to the estimation of DOD and DOA jointly for a bistatic MIMO radar by using Spatial Time-Frequency Distribution (STFD) matrices. The performance of the considered method is numerically evaluated through root mean square error (RMSE) and is compared against the conventional algorithms that do not use TF tools and as well compared against the Ćramer Rao Lower Bound (CRLB). The results show that TF based approach may be a promising candidate in terms of its robustness against channel noise. Also, the performance of the TF based DOD-DOA estimates is studied in terms of their consistency and resolvability of targets which measures the performance in a multi-target environment. Finally, the use-case of TF based estimation to solve the problem in the presence of coherent targets is analysed through simulations and inferred.

1. INTRODUCTION

Radars form a vital communication tool today, especially in military applications for detecting the presence of a target in space. In addition to its detection, its localisation is more beneficial. [1] gives an insight into the aforementioned application by exploiting the techniques of DOD-DOA estimations from target returns used in array signal processing scenarios. In doing so, the application of multistatic radars such as bistatic radars (which have non-collocated transmitters and receivers) were mandated in place of monostatic radars. Accordingly, the transmitting and receiving nodes of the radar are individually configured as an antenna array, rendering the picture of a multiple-input multiple-output (MIMO) model. For instance, when the radar transmitters and receivers are modelled as electromagnetic vector sensors (EVSs), the work in [2] presents a solution for localization of mixed targets. Also, in this context, the work in [3] presents an approach for angle estimation for arbitrary array manifolds. But the limitation of the work lies in the convergence of iterative solution as they mention. Alternatively, one can adopt subspace based direction finding techniques such as multiple signal classification (MUSIC) and estimation of signal parameters via rotational invariance technique (ESPRIT) as per literature in [4]. The work of Zheng and Chen [5] brings an algorithm by computing DOD and DOA jointly in a multi-target environment by using 2-D ESPRIT. The significance of estimating them jointly is to perform an automatic pairing between the DOD and DOA of a specific target. Marching on similar

Received 24 June 2021, Accepted 29 July 2021, Scheduled 13 August 2021

* Corresponding author: Palanisamy Ponnusamy (palan@nitt.edu).

The authors are with the Department of Electronics and Communication Engineering, National Institute of Technology, Tiruchirappalli, India.

lines, Chen et al. [6] have worked on another solution by applying singular value decomposition (SVD) to the cross correlation matrix obtained from signals received at two sub-arrays used in ESPRIT method. They claim it to be a good approach to attack spatially coloured noise scenarios. On the other hand, the work of Xie et al. in [7] demonstrates MUSIC's application to perform direction estimations for a bistatic MIMO radar in a joint fashion. Thus to include diversity of techniques for solving the problem, yet making the algorithm optimally inexpensive, a combined ESPRIT and MUSIC for DOD and DOA estimations, respectively, is adopted herein. In fact, although MUSIC incurs slightly heavy computations, it is superior to ESPRIT as it attains the Ćramer Rao Lower Bound (CRLB) and hence is efficient. It is clear that since all of the existing work as reported here employ subspace methods, their performances at low signal to noise ratios (SNRs) tend to become inconsistent. On the other hand, different approaches can be adopted to solve the considered problem using Time-Reversal (TR) based processing as in [8–10], to overcome this shortcoming. However, a better real picture of the modelling itself can be developed if the maneuvering nature of targets is included [11]. In such scenarios, by virtue of the Doppler effect's play, target returns tend to become more non-stationary, exhibiting a time-varying spectral content. Exploiting this framework of non-stationary target returns, a more novel method, and robust insight was rendered by Khan et al. [12] and Zhang et al. [13], by introducing the Time-Frequency tool for solving this direction finding problem.

The scope of this paper is to understand the role of time-frequency representations for joint DOD-DOA estimations for bistatic MIMO radar. The primary contributions of this paper are enlisted as follows. We intend to set up a framework that incorporates TF representations in a bistatic MIMO radar model and subsequently solve the direction estimation problems. We show that the considered approach is highly robust against noise and renders consistent estimates compared to its covariance matrix based counterpart, specially at low SNRs. Further, we study the resolution power of the TF-based algorithm and show that almost accurate pairing of DOD and DOA is established even at low SNRs. This is particularly interesting because, in a multi-target environment, rendering an incorrect DOD-DOA estimation can create a havoc! For example, this situation is highly intolerable in military applications. Finally, we extend the setting to a much realistic scenario by considering coherent targets. It will be justified that the approach with TF-based estimation virtually does smoothing over the target returns (due to the inherent construction of STFD matrix via averaging) and hence renders acceptable performance with coherent targets with larger probability. Additional insights on the superiority of this paper over conventional methods are elaborately indicated in Section 4 of this paper. Also, we consider the underlying channel noise as spatially white, for otherwise we can employ a pre-whitening filter using techniques like Cholesky decomposition of data STFD matrix and turn coloured noise into white. Up to the knowledge of authors, there is no work that exists in literature that has analysed the TF based direction estimation for the considered application, as much as we present in this paper.

This paper is organized as: Section 2 introduces the signal model of the Bistatic MIMO radar. Section 3 describes the theory of time-frequency analysis, its relevance in direction finding solutions and organizes the overall algorithm along with notes on computational complexities and CRLB expressions. Section 4 presents numerical results with discussions, and Section 5 marks the concluding remarks of this paper.

The notations and symbols used in this paper are as follows: All bold-uppercase letters and bold-lowercase letters denote matrices, e.g., $\mathbf{A}$, and vectors, e.g., $\mathbf{x}$; a^* denotes the complex conjugate of a; $\mathbf{A}^H$ denotes the hermitian transpose of the matrix $\mathbf{A}$; $\mathbf{A}^{-1}$ and $\mathbf{A}^\dagger$ denote the proper inverse and Moore-Penrose pseudo-inverse of the matrix $\mathbf{A}$, $\otimes$, $\odot$ and $*$ denote the matrix Kronecker, Hadamard (element-wise product), and Khatri-Rao products, respectively; $diag(\mathbf{A})$ and $diag(\mathbf{a})$ denote that column vector formed by diagonal elements of matrix $\mathbf{A}$ and diagonal matrix formed by diagonal values as elements of vector $\mathbf{a}$ respectively; $length(\mathbf{y})$ and $length(\mathbf{Y})$ represent the number of elements in vector $\mathbf{y}$ and the number of columns in matrix $\mathbf{Y}$, respectively; $\mathbb{E}[\cdot]$ denotes the statistical expectation of a random variable sampled from a random process; $\mathbf{I}_M$ denotes an identity matrix of order M; λ denotes the wavelength of the incoming signal; $\|\cdot\|$ denotes the l_2 norm; and $\lfloor\cdot\rfloor$ denotes the floor function. Finally, $Re(\cdot)$ takes the real part of $(\cdot)$; $\frac{\partial(\cdot)}{\partial x}/\frac{d(\cdot)}{dx}$ take the partial/full derivative w.r.t x; and $\mathbf{x} \sim \mathcal{CN}(\mathbf{a}, \mathbf{B})$ denotes that $\mathbf{x}$ is a circular symmetric complex Gaussian random vector with mean $\mathbf{a}$ and covariance matrix $\mathbf{B}$.

2. BISTATIC MIMO RADAR — SIGNAL MODEL

The geometrical setup of a bistatic MIMO radar is portrayed in Figure 1 with the DOD and DOA for k^{th} target. As shown in the figure, let the transmitter and receiver be modeled as N_T-element uniform linear array (ULA) and N_R-element ULA, respectively. We assume that the knowledge of source enumeration is known a priori through target detections or similar techniques[†]. In fact, source enumeration of non-stationary targets itself can be a separate problem. Let there be P number of targets present in far-field distant space, each exhibiting constant oscillatory motion about a mean position. Further, both the transmitting and receiving arrays are assumed to have uniform inter-elemental distances, d.

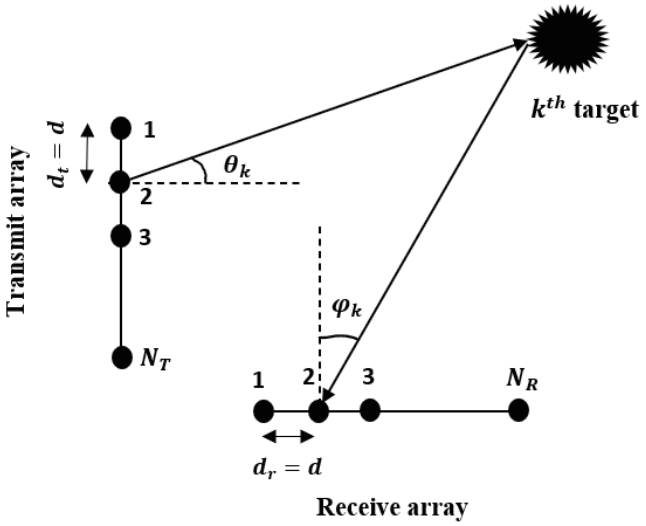

Figure 1. Bistatic MIMO Radar setup.

Also, each target is characterized by its reflection coefficient. However, owing to the assumption made on the target to be in motion, the reflection coefficient is also assumed to vary in time because of the play of doppler effect. From the foregoing analysis, it is clear that the reflected signals possess a time varying spectral characteristic which encourages a time-frequency processing of these signals at the receiving array. Let the reflection coefficient of l^{th} target at time t be modelled as $\gamma_l(t) = \rho_l(t)e^{j2\pi f_{d,l}(t)t}$ where ρ denotes the magnitude of reflection coefficient (which describes the radar cross-section), and $f_d(t)$ denotes the instantaneous doppler shift frequency at time t. Recollect the fact that, in radar processing problems, series of pulses are transmitted once in every fixed interval, called as Pulse Repetition Period (PRP). So, there are two types of variables defined in the domain of time, namely the PRP and the sampling time of the pulses, which exists within the pulse. Hence for the sake of distinction, as per [13], let the former be termed as the slow time domain indexes t and the latter as fast time domain indexes, $\frac{t}{T}$, where T is the number of samples in a pulse. Hence, for every t units of time, T snapshots are received.

Thus, the complex baseband received signal matrix $\mathbf{X}(t) \in \mathbb{C}^{N_R \times T}$ for a collection of T snapshots at time t, at the receive array can be written as:

$$\mathbf{X}(t) = \mathbf{A_r}\mathbf{\Gamma}(t)\mathbf{A_t}^H\mathbf{S} + \mathbf{N}(t) \tag{1}$$

where $\mathbf{A_t} \in \mathbb{C}^{N_T \times P}$ and $\mathbf{A_r} \in \mathbb{C}^{N_R \times P}$ are the complex transmitting and receiving array steering matrices, respectively. If the transmitting and receiving array steering vectors, denoted by $\mathbf{a_t}(\theta)$ and $\mathbf{a_r}(\phi)$, are given by:

$$\mathbf{a_t}(\theta) = \left[1, \quad e^{-j\omega\frac{dsin(\theta)}{c}} \quad , \ldots\ldots, e^{-j(N_T-1)\omega\frac{dsin(\theta)}{c}}\right]^T \tag{2}$$

[†] However, one naive approach for source enumeration is to count the dominant eigen values of STFD matrix after estimating noise variance and hence estimate the number of sources. More efficient techniques can be included as in [22]. However, this approach may not work when targets are coherent. In such cases, a more generalized and relevant approach is solved in [23].

and

$$\mathbf{a_r}(\phi) = \left[1, \quad e^{-j\omega\frac{dsin(\phi)}{c}} \quad , \ldots\ldots, e^{-j(N_R-1)\omega\frac{dsin(\phi)}{c}}\right]^T, \tag{3}$$

it can be written that $\mathbf{A_t} = [\mathbf{a_t}(\theta_1), \quad \mathbf{a_t}(\theta_2), \ldots, \mathbf{a_t}(\theta_P)]$ and $\mathbf{A_r} = [\mathbf{a_r}(\phi_1), \quad \mathbf{a_r}(\phi_2), \ldots, \mathbf{a_r}(\phi_P)]$. Further $\mathbf{S} \in \mathbb{C}^{N_T \times T}$ is an orthogonal matrix ($\mathbf{SS}^H = \mathbf{I}$), representing the emission of T narrow band snapshots from N_T antennas. Finally, $\mathbf{\Gamma}(t) \in \mathbb{C}^{P \times P}$ represents a complex diagonal matrix with elements as the individual targets' reflection coefficient at time t and is given by:

$$\mathbf{\Gamma}(t) = \text{diag}(\boldsymbol{\gamma}(t))$$

where $\boldsymbol{\gamma}(t) = [\gamma_1(t), \gamma_2(t), \ldots, \gamma_P(t)]^T$. Subsequently, as in conventional radar detection, the received signal is passed through a matched filter. This operation is accomplished by post multiplying Eq. (1) by $\mathbf{S}^H$ on both sides. By noticing $\mathbf{SS}^H = \mathbf{I}$, the resultant equation turns out to be:

$$\mathbf{Y}(t) = \mathbf{A_r}\mathbf{\Gamma}(t)\mathbf{A_t}^H + \mathbf{Z}(t) \tag{4}$$

where $\mathbf{Y}(t) = \mathbf{X}(t)\mathbf{S}^H \in \mathbb{C}^{N_R \times N_T}$ and $\mathbf{Z}(t)$ is the filtered noise. Vectorizing this obtained equation by stacking all the column vectors one below the other,

$$\mathbf{y}(t) = \mathbf{w}(t) + \mathbf{z}(t) = \mathbf{A}\boldsymbol{\gamma}(t) + \mathbf{z}(t) \tag{5}$$

where $\mathbf{z}(t) \sim \mathcal{CN}(\mathbf{0}, \mathbf{I}_{N_R N_T})$ is the additive white Gaussian noise (AWGN), and $\mathbf{A} \in \mathbb{C}^{N_T N_R \times P}$ is the effective steering matrix and can be proved to be given by:

$$\mathbf{A} = \mathbf{A_t} * \mathbf{A_r} = [\mathbf{a_{t},1} \otimes \mathbf{a_{r},1}, \mathbf{a_{t},2} \otimes \mathbf{a_{r},2}, \ldots, \mathbf{a_{t},P} \otimes \mathbf{a_{r},P}] \tag{6}$$

Here, $\mathbf{a_t}$ and $\mathbf{a_r}$ are consistent with the definitions made earlier. It can be noted that, in Eq. (5), $\mathbf{y}$ can be treated like a virtual snapshot for the virtual ULA with $M \triangleq N_T N_R$ elements [5, 13].

3. TIME-FREQUENCY REPRESENTATIONS AND APPLICATION IN DOD-DOA ESTIMATIONS

3.1. Time-Frequency Representations

Time-Frequency (TF) representations is a very popular tool used in the regime of non-stationary signal processing. In this analysis, the spectral characteristics are studied repeatedly at different distinct instants of time. An elementary procedural technique of such kind includes short-time Fourier transforms. Although it is an effective tool for conceptualizing non-stationarity, it is a linear transform. To improve the signal concentration while estimating the spectral components at the time instant of interest, higher order TF representations are sought [14]. In doing so, the work done by Cohen [15] gives a general representation of higher order TF Distributions (TFD). In this paper, we use a quadratic — TFD, namely Wigner-Ville Distributions (WVD). More formally, the Cohen's class of auto-term quadratic TF Distributions (TFD) of a discrete signal $x(t)$ is given by:

$$D_{xx}(t,f) = \sum_{u=-\infty}^{u=\infty} \sum_{\tau=-\infty}^{\tau=\infty} g(u,\tau)x(t+u+\tau)x^*(t+u-\tau)e^{-j4\pi f\tau} \tag{7}$$

where $g(u,\tau)$ is a kernel function that decides the type of distribution considered. For WVD, $g(u,\tau) = \delta(u)w(\tau)$ where $w(\tau)$ is a window function (e.g., rectangular window). Thus, WVD is computed by:

$$D_{xx}(t,f) = \sum_{\tau=-\infty}^{\tau=\infty} x(t+\tau)x^*(t-\tau)e^{-j4\pi f\tau} \tag{8}$$

From the above expression it can be inferred that the term inside the summation is essentially the evaluation of auto-correlation of $x(t)$ but for the summation of values over the entire range of time. Instead, an outer summation is performed over the entire range of $\tau \in (-\infty, +\infty)$ representing different time lags. Hence, this correlation which is not summed over the entire running time index t, rather summed up w.r.t τ, is a measure of localized correlation value at time instant t. This is

the local auto correlation defined around the neighbourhood region around t of radius τ and given as: $R(t,\tau) = x(t+\tau)x^*(t-\tau)$. Further, a more feasible term called Pseudo-WVD (PWVD) is rather constructed consisting of finite H samples only. Thus the expression for computing PWVD boils down to:

$$D_{xx}(t,f) = \sum_{\tau=-(\frac{H-1}{2})}^{\tau=(\frac{H-1}{2})} x(t+\tau)x^*(t-\tau)e^{-j4\pi f\tau} \tag{9}$$

Alternatively, WVD (PWVD) is a way of visualizing how the Power Spectral density (PSD) (or energy spectral density for deterministic energy signals) varies with time. Similarly one can define WVD between two different signals. Eq. (9) deals with TFD for a single-channel signal, and an extension of it can be made for a multi-channel signal. In such a case, application of Eq. (9) turns out to be a square matrix, referred to as Spatial Time-Frequency Distribution (STFD) Matrix. Thus, we have,

$$\mathbf{D_{xx}}(t,f) = \sum_{\tau=-(\frac{H-1}{2})}^{\tau=(\frac{H-1}{2})} \mathbf{x}(t+\tau)\mathbf{x}^H(t-\tau)e^{-j4\pi f\tau} \tag{10}$$

It should be noted that the construction of these matrices over appropriate (t,f) points would prove to be beneficial by enhancing the SNR of the signal [17]. For instance, if the chirp signal of frequency f_1 arrives at the receiver sensor in time neighborhood of $t = t_1$, then $\mathbf{D_{xx}}(t_1, f_1)$ would prove to be beneficial in capturing the information of this chirp's signature effectively. Reference [16] very clearly lists down the merits of the application of STFD matrices, and an important artifact that arises out of Eq. (10) is the generation of cross-terms, which describes the interaction of inter-channel signals. Since such cross terms lead to misinterpretation of actual signals' behavior, smoothing method such as averaging the STFD matrices is carried out, which proves to diminish the cross terms due to their oscillatory nature [13, 14].

3.2. Joint DOD-DOA Estimation Using TF-Analysis

This subsection deals with the application of STFDs in direction finding problems in radar applications. Before proceeding any further, an intuition behind the proof of applicability of STFDs in direction finding is discussed. By employing Eq. (5) in Eq. (10), it can be found that,

$$\mathbf{D_{yy}}(t,f) = \mathbf{A}\mathbf{D_{\gamma\gamma}}(t,f)\mathbf{A}^H + \mathbf{A}\mathbf{D_{\gamma z}}(t,f) + \mathbf{D_{z\gamma}}(t,f)\mathbf{A}^H + \mathbf{D_{zz}}(t,f). \tag{11}$$

In the above expression, the first term in RHS represents the contribution from target returns, while second and third terms denote the interaction between the target returns and noise. The last term is the auto-term of noise vector. It should be recalled that the STFD matrix has to be constructed only in those (t,f) points which lie in the target returns' Doppler signature following an instantaneous frequency (IF) law. Under the assumptions that signal and noise vectors are independent with noise being modeled as a zero-mean white vector, it can be deduced from Eq. (11) that,

$$\mathbb{E}[\mathbf{D_{yy}}(t,f)] = \mathbf{A}\mathbf{D_{\gamma\gamma}}(t,f)\mathbf{A}^H + \sigma_n^2\mathbf{I}_{N_TN_R}. \tag{12}$$

It should be simultaneously observed that if Eq. (5) is used for constructing the auto-correlation matrix instead of an STFD matrix, a similar equation can be obtained as:

$$\mathbf{R_{yy}} = \mathbf{A}\mathbf{R_{\gamma\gamma}}\mathbf{A}^H + \sigma_n^2\mathbf{I}_{N_TN_R} \tag{13}$$

Thus, Eqs. (12) and (13) look very similar, and hence, it can be inferred that STFD matrix and auto-correlation matrix are equivalent in a statistical sense.

As a consequence, subspace spanned by the principle eigenvectors of $\mathbf{D_{yy}}$ over the selected and relevant (t,f) points will be the same as the space spanned by those column vectors of $\mathbf{A}$ whose corresponding target returns were identified in the same selected (t,f) points. Thus, it can be concluded that time-frequency representations by means of an STFD operator is very useful for direction finding problems with in fact added advantages as discussed in [17]. Formally, delving into the algorithm, a joint estimation of DOD and DOA is sketched using combined ESPRIT and MUSIC, respectively. In

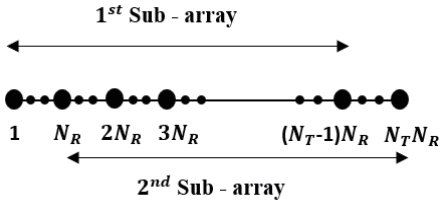

Figure 2. virtual sub-array configuration for TF-ESPRIT.

fact, a time-frequency based ESPRIT is foremostly performed to estimate the DOD of targets followed by which DOAs of targets are estimated using time-frequency MUSIC with the estimated DOD of the corresponding target as input. Hence, an automatic pairing between the DOD and DOA is established.

Thus, for a case of P target returns over the selected region of (t, f) points, ESPRIT is performed by partitioning the virtual ULA into two sub-arrays. Taking insights from [17], let the sub-array setup be configured as shown in Figure 2, i.e., while first $(N_T - 1)N_R$ antennas constitute the 1^{st} sub-array-with steering matrix, $\mathbf{A_1} \triangleq \mathbf{A'_t} * \mathbf{A_r}$; the last $(N_T - 1)N_R$ antennas constitute the 2^{nd} sub-array-with steering matrix, $\mathbf{A_2} \triangleq \mathbf{A''_t} * \mathbf{A_r}$ where $\mathbf{A'_t}$ and $\mathbf{A''_t}$ are matrices obtained by retaining first and last $N_T - 1$ rows of $\mathbf{A_t}$ respectively. Accordingly, let the final expression which governs the angle estimation via ESPRIT be formulated as:

$$\mathbf{\Psi T} = \mathbf{T\Omega} \tag{14}$$

with

$$\mathbf{\Psi} = \left(\mathbf{U_{S,1}}^H \mathbf{U_{S,1}}\right)^{-1} \mathbf{U_{S,1}}^H \mathbf{U_{S,2}} \tag{15}$$

and

$$\mathbf{\Omega} = \mathrm{diag}(\{\exp(-j2\pi d \sin(\theta_k)/\lambda)\}_{k=1}^{k=P}) \tag{16}$$

where $\mathbf{U_{S,1}}$ and $\mathbf{U_{S,2}}$ are signal sub-space bases for the two sub-arrays respectively with $\mathbf{Q}$ being an arbitrary linear transform. Further, since Eq. (14) instantiates the fact that non-zero elements of $\mathbf{\Omega}$ are the eigen values of $\mathbf{\Psi}$, a further simplification can be obtained as:

$$\mathbf{\Lambda_\Psi} = \mathrm{diag}(\{\exp(-j2\pi d \sin(\theta_k)/\lambda)\}_{k=1}^{k=P}) \tag{17}$$

where $\mathbf{\Lambda_\Psi}$ is the diagonal matrix with elements as eigen values of $\mathbf{\Psi}$.

Thus, DOD of P targets can be computed conveniently using Eq. (17). In order to compute the DOA of P targets, the TF-MUSIC spectrum is derived for k^{th} target ($\forall k \in \{1, 2, \ldots, P\}$) as follows.

$$\mathbf{P}(\phi) = \frac{1}{\mathbf{a_r}^H(\phi)[\mathbf{a_t}(\theta_k) \otimes \mathbf{I}_{N_R}]^H \mathbf{U_N} \mathbf{U_N}^H [\mathbf{a_t}(\theta_k) \otimes \mathbf{I}_{N_R}] \mathbf{a_r}(\phi)} \tag{18}$$

$$= \frac{1}{||\{[\mathbf{a_t}(\theta_\mathbf{k}) \otimes \mathbf{I_{N_R}}]\mathbf{a_r}(\phi)\}^\mathbf{H} \mathbf{U_N}||^2} \tag{19}$$

where $[\mathbf{a_t}(\theta_k) \otimes \mathbf{I}_{N_R}]\mathbf{a_r}(\phi) = k^{th} col.\ \mathbf{A_t} * \mathbf{A_r}|_{\theta=\widehat{\mathbf{DOD}}(k)}$, $\mathbf{U_N}$ is the corresponding noise-subspace and ϕ running from $-\frac{\pi}{2}$ to $\frac{\pi}{2}$. The argument of this function, which renders a peak, is obtained as the DOA of k^{th} target. Thus, the overall algorithm can be formulated as shown in *Algorithm 1*.

3.2.1. Computational Complexity Analysis

Following notations are additionally introduced to make the description succinct. Let the number of frames and frame length used in computing STFD matrices be N_{SF} and N_F, respectively. Let the precision requirement in computation of instantaneous frequency and direction estimation in the grid search of MUSIC algorithm be P_I and P_{DE}, respectively. Table 1 gives the computational complexity compendiously, in terms of the number of multiplications and additions to evaluate *Algorithm 1*.[‡]

[‡] This algorithm was executed on MATLAB 2020a version. Hence, the computational complexities are described according to MATLAB documentation of certain inbuilt functions. For example, the complexity of eigen decomposition is described based on QR iterative algorithms. We also assume trigonometric, exponential/log functions to be evaluated using AM-GM mean iterations.

Algorithm 1: Joint DOD-DOA estimation of P targets using Time-Frequency ESPRIT & MUSIC for bistatic MIMO Radar

Input: Array snapshots:$\mathbf{Y} = [\mathbf{y_1}, \ldots, \mathbf{y_T}]$; Transmit & Receive array steering matrices: $\mathbf{A_t}$,$\mathbf{A_r}$
Output: DOD and DOA of P targets

Initialize the $t-f$ point resolution, *tf_res* $\leftarrow$ 150 samples; overlapping ratio, *ovlp_rat* $\leftarrow$ 0.5.
Let *eff_frm_len* = *tf_res* $\times$ *ovlp_rat*.
`/* Module 1: Construction of STFD matrices */`
Set *sample_len* $\leftarrow \lfloor \frac{\text{length}(\mathbf{Y})}{\textit{eff\_frm\_len}} \rfloor - 1$.
for *i* $\leftarrow$ *1 to length*($\mathbf{Y}$) *in steps of eff_frm_len* **do**
    $l \leftarrow i$ *to* $i+$ *tf_res*
    if $\mathbf{y}(l)$ *is real* **then**
        $\mathbf{x} \leftarrow \mathbf{y}(l) + j\tilde{\mathbf{y}}(l)$; $\tilde{\mathbf{y}}$ = Hilbert transform$\{\mathbf{y}\}$
    else
        $\mathbf{x} \leftarrow \mathbf{y}(l)$
    Compute instantaneous frequency, $f_i \leftarrow \frac{1}{2\pi}\frac{d\phi_{\mathbf{x}}}{dt}$; $\phi_{\mathbf{x}} \triangleq$ phase of $\mathbf{x}$.
    $\mathbf{STFD_{iter}}(i) \leftarrow \sum_{k=i-0.5*tf\_res}^{k=i+0.5*tf\_res} \mathbf{x}(i-k)\mathbf{x}^H(i+k)e^{-j4\pi f_i k}$
$\widehat{\mathbf{STFD}} = \frac{1}{sample\_len}\sum_{i=1}^{sample\_len} \mathbf{STFD_{iter}}(i)$; `// Averaging`
`/* Module 2: Eigen Decomposition of STFD */`
Perform Eigen decomposition of $\widehat{\mathbf{STFD}}$: $(\mathbf{\Lambda}, \mathbf{U})$.
Select the P dominant eigen vectors to form a basis for signal sub-space, $\mathbf{U_S}$.
Select the rest $M-P$ eigen vectors to form a basis for noise sub-space, $\mathbf{U_N}$.
Initialize the DOD and DOA estimates : $\widehat{\mathbf{DOD}} \leftarrow [\,]$, $\widehat{\mathbf{DOA}} \leftarrow [\,]$.
Initialize MUSIC step resolution, $angle_{res}$.
Compute the effective array steering matrix, $\mathbf{A} \leftarrow \mathbf{A_t} * \mathbf{A_r}$, as per (6).
`/* Module 3: DOD (θ) Estimation using TF ESPRIT */`
Compute the transformation matrix, $\mathbf{Q} \leftarrow \mathbf{A}^{\dagger}\mathbf{U_S}$.
Determine the sub-steering matrices: $\mathbf{A_1} \leftarrow \mathbf{A'_t} * \mathbf{A_r}$ and $\mathbf{A_2} \leftarrow \mathbf{A''_t} * \mathbf{A_r}$.
Compute the sub-space bases: $\mathbf{U_{S,1}} \leftarrow \mathbf{A'_t Q}$, $\mathbf{U_{S,2}} \leftarrow \mathbf{A''_t Q}$.
Obtain $\mathbf{\Psi} \leftarrow \mathbf{U_{S,1}}^{\dagger}\mathbf{U_{S,2}}$.
Compute the eigen values of $\mathbf{\Psi}$ as $\xi_1, \xi_2, \xi_3, \ldots, \xi_P$.
for $k \leftarrow 1$ *to* P **do**
    $\xi_k \leftarrow e^{-j2\pi\frac{d\sin\theta_k}{\lambda}}$.
    $\widehat{\mathbf{DOD}}(k) \leftarrow \theta_k = \sin^{-1}(|\frac{log(\xi_k)\lambda}{-j2\pi d}|)$.
`/* Module 4: DOA (φ) Estimation using TF MUSIC */`
for $k \leftarrow 1$ *to* P **do**
    for $\phi \leftarrow -\frac{\pi}{2}$ *to* $\frac{\pi}{2}$ *in steps of* $angle_{res}$ **do**
        $\mathbf{a} \leftarrow k^{th}$ *col.* $\mathbf{A_t} * \mathbf{A_r}\Big|_{\theta=\widehat{\mathbf{DOD}}(k)} = [\mathbf{a_t}(\theta_k) \otimes \mathbf{I}_{N_R}]\mathbf{a_r}(\phi)$.
        $\mathbf{P_{spec}}(k,\phi) \leftarrow \frac{1}{\mathbf{a_r}^H(\phi)[\mathbf{a_t}(\theta_k)\otimes\mathbf{I}_{N_R}]^H\mathbf{U_N}\mathbf{U_N}^H[\mathbf{a_t}(\theta_k)\otimes\mathbf{I}_{N_R}]\mathbf{a_r}(\phi)} = \frac{1}{||\{[\mathbf{a_t}(\theta_k)\otimes\mathbf{I_{N_R}}]\mathbf{a_r}(\phi)\}^{\mathbf{H}}\mathbf{U_N}||^2}$
    $\widehat{\mathbf{DOA}}(k) \leftarrow \underset{\phi}{\text{argmax}}\mathbf{P_{spec}}(k)$
$\widehat{\mathbf{DOD}}$ & $\widehat{\mathbf{DOA}}$ form the pairwise ordered estimations.

Table 1. Computational complexity.

Steps	Complexity
Module 1: Construction of STFD matrix	
Computation of instantaneous frequency	$\mathcal{O}(N_F^2 P_I \log P_I)$
STFD matrix construction	$\mathcal{O}(M + N_{SF}M^2 + M^2)$
Module 2: Eigen analysis of STFD matrix	
Eigen value decomposition	$\mathcal{O}(M^3)$
Module 3: TF-ESPRIT	
Computation of $\mathbf{A}, \mathbf{Q}$	$\mathcal{O}(2MP + 3MP^2)$
Computation of $\mathbf{A_1}$, $\mathbf{A_2}$	$\mathcal{O}(2(M - N_R)P)$
Computation of $\mathbf{U_{S,1}}$, $\mathbf{U_{S,2}}$	$\mathcal{O}(4(M - N_R)P^2)$
Computation of $\mathbf{\Psi}$	$\mathcal{O}((M - N_R)(P^2 + 2(M - N_R - P)P))$
Eigen value decomposition	$\mathcal{O}(P^3)$
DOD estimation	$\mathcal{O}(\frac{P^2}{2} + \frac{P}{2})$
Module 4: TF-MUSIC	
Computation of $\mathbf{U_N U_N^H}$	$\mathcal{O}(2(M - P)M^2)$
Computation of MUSIC spectrum	$\mathcal{O}(M^2 + M + 2MN_R)$
Computation of P peaks (DOA estimation)	$\mathcal{O}(4PP_{DE})$

Thus, the overall complexity can be obtained by taking the sum of all individual complexities. We also compare the algorithm considered in this work against conventional covariance matrix approaches in terms of the underlying complexity of implementation. The difference lies in the module of constructing STFD matrices over covariance matrices. While the former requires $\mathcal{O}(N_F^2 P_I \log P_I + M + N_{SF}M^2 + M^2)$ computations, the latter requires $\mathcal{O}(TM^2 + M^2)$. In practice, we have $N_{SF} < T$ and $N_F \ll T$. This is because in order to estimate the instantaneous frequency, frame length is kept much smaller than the total number of samples. Overall, the complexity of TF based solution can be made comparable with that of existing conventional solutions, yet deriving numerous robustness over existing solutions as will be shown numerically in next section.

3.2.2. Discussion of the Ćramer Rao Lower Bound (CRLB)

In this subsection, the Ćramer Rao Lower Bound (CRLB) for DOD-DOA estimates is computed, which will be useful in the next section, to obtain a benchmark against which we evaluate the performance of TF-based estimates. To this end, using Eq.'(B.6.32) of Appendix B in [18], it is straightforward to show that, for $\mathbf{\Theta} \triangleq [\theta_1, \phi_1, \theta_2, \phi_2, \ldots, \theta_P, \phi_P]^T \in \mathbb{R}^{2P\times 1}$,

$$\text{CRLB}(\mathbf{\Theta}) = \frac{\sigma^2}{2N}\left\{Re\left[\mathbf{D^H \Pi_A^{\perp} D} \odot (\hat{\mathbf{R}}^{\mathbf{T}} \otimes \mathbf{I_2})\right]\right\}^{-1}$$

where $\{\theta_i\}_{i=1}^P$ and $\{\phi_i\}_{i=1}^P$ denote the DOD and DOA of P targets, respectively; N is the number of pulses transmitted (across slow time indices), $\boldsymbol{D} = [\boldsymbol{d}(\theta_1), \boldsymbol{d}(\phi_1), \ldots, \boldsymbol{d}(\theta_P), \boldsymbol{d}(\phi_P)] \in \mathbb{C}^{N_t N_r \times 2P}$ such that $\boldsymbol{d}(\theta_i) = \frac{\partial(\boldsymbol{a}_t(\theta_i) \otimes \boldsymbol{a}_r(\phi_i))}{\partial(\theta_i)}$ and $\boldsymbol{d}(\phi_i) = \frac{\partial(\boldsymbol{a}_t(\theta_i) \otimes \boldsymbol{a}_r(\phi_i))}{\partial(\phi_i)}$, $\boldsymbol{\Pi}_{\boldsymbol{A}}^{\perp} = \boldsymbol{I} - \boldsymbol{\Pi}_{\boldsymbol{A}}$ with $\boldsymbol{\Pi}_{\boldsymbol{A}} = \boldsymbol{A}\left(\boldsymbol{A}^H \boldsymbol{A}\right)^{-1} \boldsymbol{A}^H$ and finally $\hat{\boldsymbol{R}} = \frac{1}{N}\sum_{k=1}^{N} \boldsymbol{\gamma}(k)\boldsymbol{\gamma}^H(k) \in \mathbb{C}^{P\times P}$. Thus when all DODs and DOAs are totally independent,

$$\text{CRLB (DOD)} = \sum_{i=1}^{P} [\text{CRLB}(\mathbf{\Theta})]_{2i-1,2i-1} \tag{20}$$

and

$$\text{CRLB (DOA)} = \sum_{i=1}^{P} [\text{CRLB}(\boldsymbol{\Theta})]_{2i,2i} \tag{21}$$

4. NUMERICAL RESULTS AND DISCUSSIONS

The following initializations have been adopted in this paper for evaluating the numerical results. Let $P = 2$, and Walsh-Hadamard codes are used as radar transmitting waveforms. Transmitting and receiving ULAs are assumed to have 4 and 5 antennas each with identical inter elemental spacing, $d = d_t = d_r = \frac{\lambda}{2}$. Further, the target properties are summarized in Table 2.

Table 2. Target properties.

Target #	**Properties**			
	DOD (deg)	***DOA (deg)***	***Doppler shift (Hz)***	$\lvert\gamma(t)\rvert$
Target 1	10	60	0.05-0.35	0.75
Target 2	65	20	0.15-0.45	0.5

Furthermore, we assume $N = 1000$ pulse transmission with 1024 samples per pulse.

Figures 3 and 4 depict the non-stationary instantaneous spectral content of target returns (at SNR = 20 dB) using short time Fourier transform and pseudo Wigner-Ville distributions, respectively. Thus, it is clear that higher order TFDs such as PWVD gives better spectral concentration than linear transforms. However, the limitation of the latter is the generation of cross terms as seen in Figure 4. However, its contribution is less intense due to the averaging step during the construction of STFD matrices. Figure 5 shows the Joint DOD-DOA estimation in a paired manner at SNR = 0 dB after averaging over 100 Monte-Carlo simulations. As seen, estimated value and theoretical values match very well up to experimental requirements. Thus, even at lower SNRs, TF-based DOD & DOA estimations are performing better.

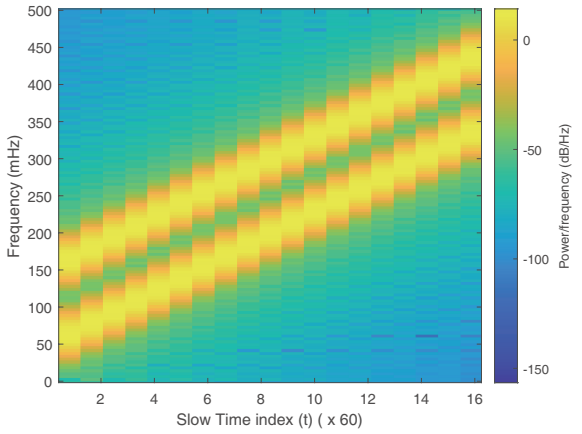

Figure 3. STFT of target returns.

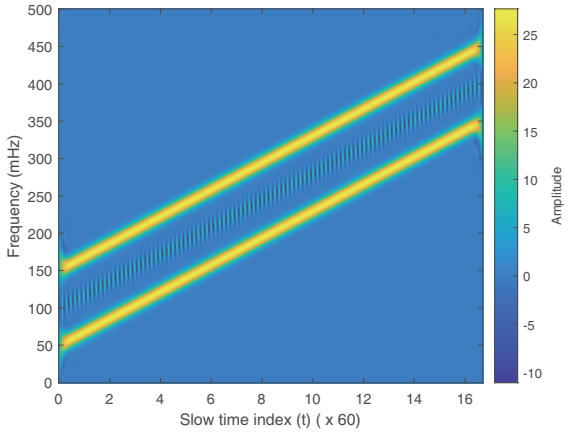

Figure 4. PWVD of target returns.

In Figures 6 and 7, the performance of the TF based DOD and DOA estimates in terms of RMSE is analysed against the conventional non TF based estimates and the CRLB after performing 100 Monte-Carlo simulations. It is evident that the RMSE of non TF based estimates are uniformly lower bounded by the TF based estimates, over a range of SNRs. Also, TF based DOA estimate attains the CRLB

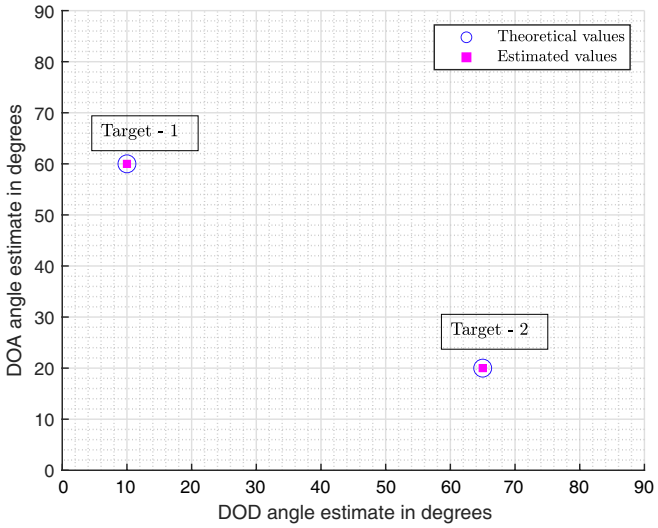

Figure 5. DOD-DOA estimates.

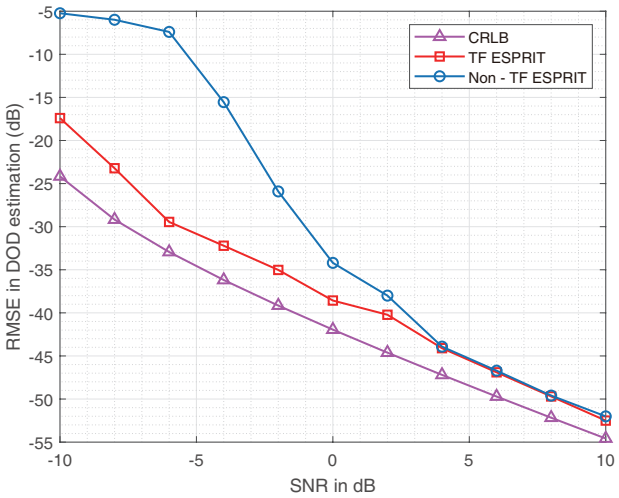

Figure 6. RMSE: DOD estimate vs SNR.

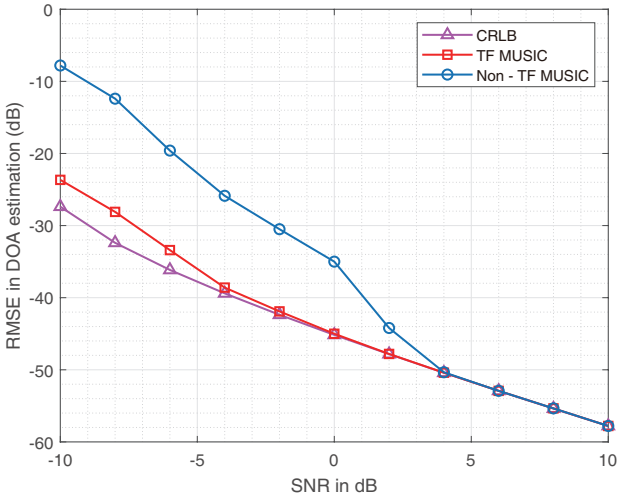

Figure 7. RMSE: DOA estimate vs SNR.

very quickly compared to that of non TF based DOA estimate, thus becoming efficient quickly. This illustrates the usefulness of TF tools for direction finding of signals with non-stationary signatures. However, it is observed that TF based DOD estimator does not attain CRLB although the RMSE of non TF based DOD estimate is lower bounded by its TF based counterpart. This is because of the underlying method of ESPRIT which hardly becomes efficient at lower SNRs [19].

In Figures 8 and 9, the consistency of the TF based DOA estimates of 2 targets are studied at low SNR. For an experiment operating at SNR $= -20$ dB with 15 Monte Carlo (MC) runs, the spatial pseudo spectrum of TF MUSIC is plotted and overlayed in the figures. It is observed that even for SNR as low as -20 dB, estimates in all the MC runs cluster to around the true angle, without any ambiguity in pairing. Thus, the estimates are found to be consistent.

In Figures 10 and 11, the resolving capability of the estimates is investigated, i.e., the extent, to which the TF based estimates are able to resolve the two targets distinctly even when they are in close vicinity, is analysed. This aspect is worth studying because of its ability to closely dictate the accuracy of DOD-DOA pairing when multiple targets are present within the range of the radar. For the purpose of illustration, the difference in theoretical DOAs is gradually increased from 0.1° to 10°, and

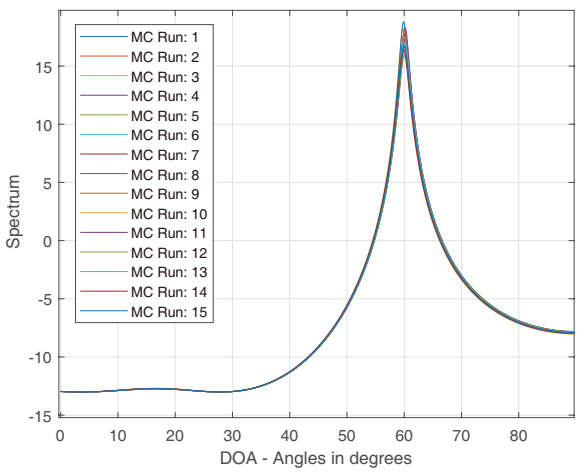

Figure 8. MUSIC spectrum: Target-1.

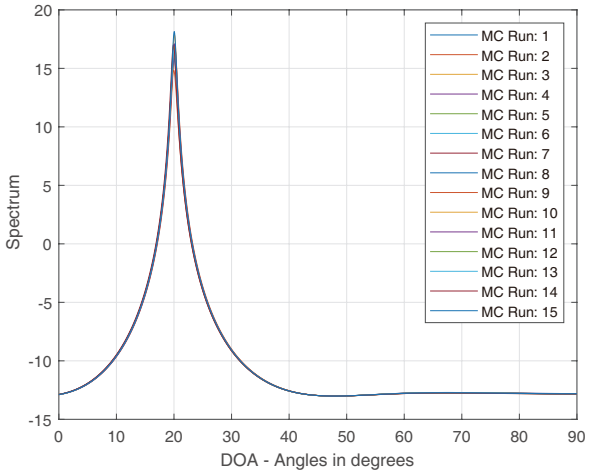

Figure 9. MUSIC spectrum: Target-2.

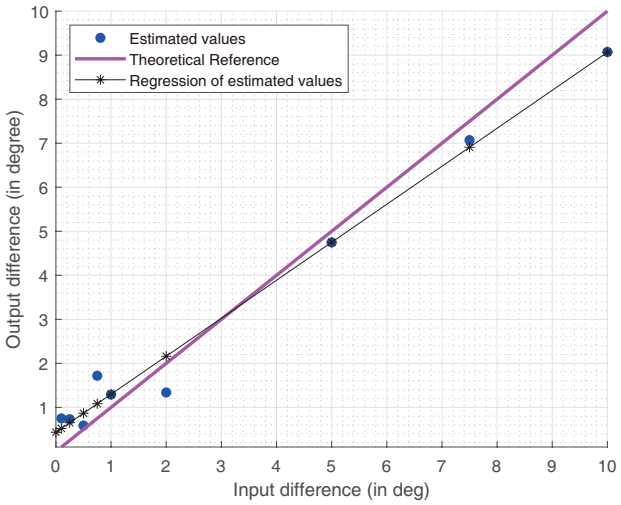

Figure 10. Resolvability; SNR $= -10$ dB.

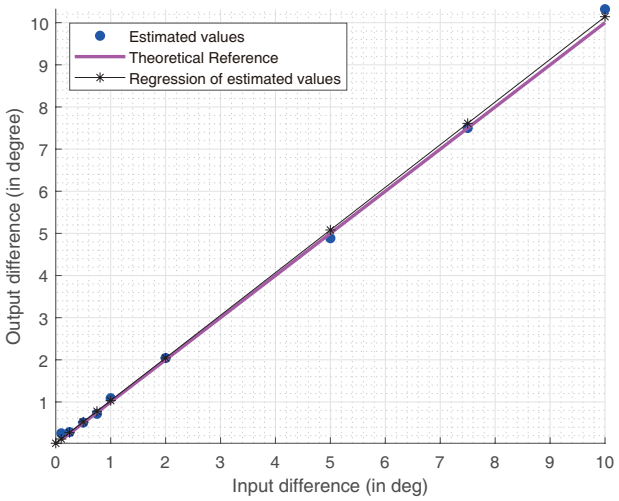

Figure 11. Resolvability; SNR $= 0$ dB.

the estimated difference between the DOAs is tracked and analysed. As depicted, the linear regression line obtained with finite set of measurements converges to the theoretical reference as SNR increases. Even at lower SNRs say, at -10 dB, the performance is appreciable, which corroborates the RMSE plots obtained in Figures 7 and 6.

Finally, we also study the scope of TF based direction estimation when targets are coherent. In such scenarios, it is known that conventional subspace methods cannot be directly employed to solve the problem due to inherent rank deficiency of source covariance matrix. In order to study the performance using TF methods numerically, several trials of TF-MUSIC spectrums for a degree of coherence of 0.9 between the targets are obtained and overlayed on the same plots for each target at varying SNRs. The relevant plots are shown in Figures 12(a) abd 12(b) at 0 dB SNR and in Figures 12(c) and 12(d) at 20 dB SNR. It is seen that the peaks are not very sharp even at high SNRs, hence the algorithm may not be successful for very closely spaced coherent targets. However, for reasonably widely spaced targets, an approximate estimate of DOA can be determined. However, it is interesting to see that, even at an SNR as low as 0 dB, the angle estimation is optimal up to an order of permutation of approximate DOA values of the two targets. This is a straightforward consequence of the underlying targets to be coherent: where although the likelihood of the algorithm to miss the true DOA is small, it

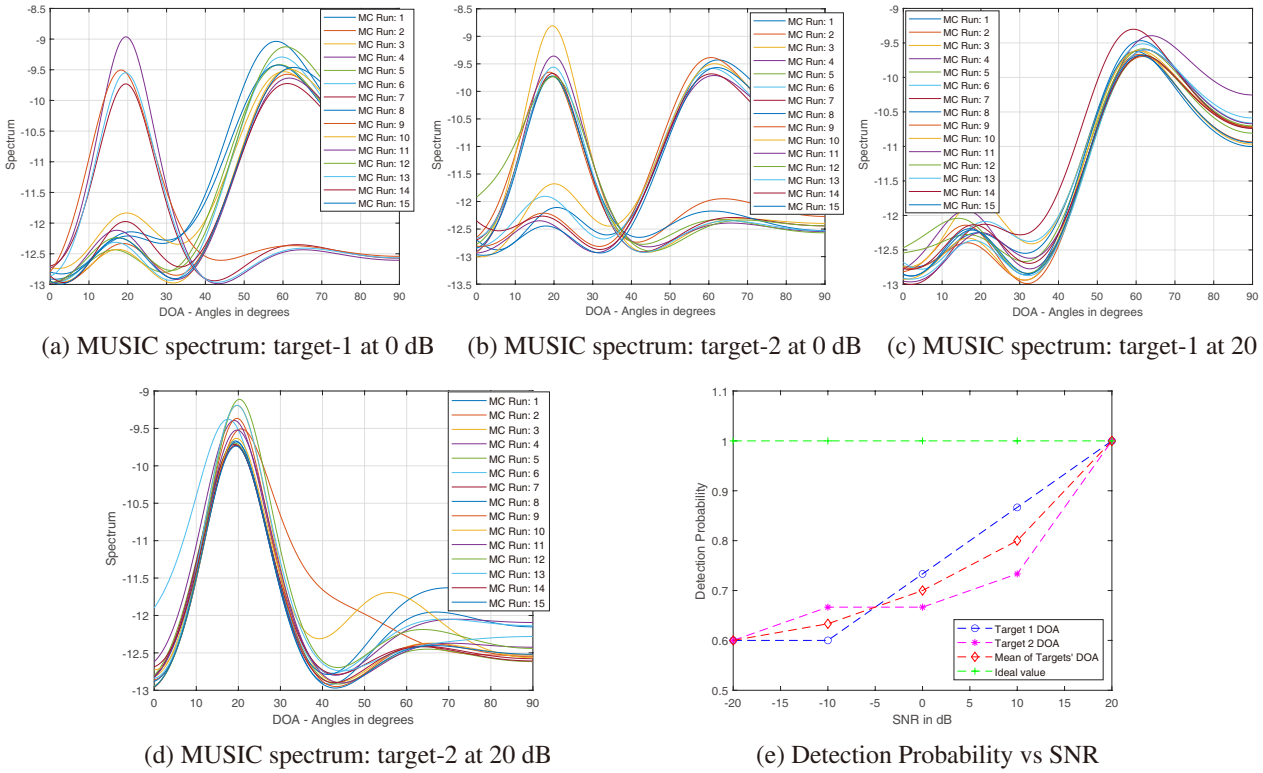

(a) MUSIC spectrum: target-1 at 0 dB (b) MUSIC spectrum: target-2 at 0 dB (c) MUSIC spectrum: target-1 at 20 dB

(d) MUSIC spectrum: target-2 at 20 dB (e) Detection Probability vs SNR

Figure 12. Performance of TF based direction estimation for Coherent targets.

is non-trivial! Thus, the algorithm does not report any spurious angles as opposed to what conventional non-TF based algorithms would render. The rationale behind this observation can be justified by the following. Constructing STFD matrices at different TF points may be looked as a way of performing spatial smoothing [20] (or Polarization Difference Smoothing when Bistatic MIMO Radar is configured with EVSs [21]): for example we may obtain different independent snapshots, when they are measured at different independent points in TF grid, which when being collected as a whole and combined, may potentially improve the rank, a direct analogy to the measurement of samples at different points in space in spatial smoothing [20]. Thus, the TF based solution can render as good solutions as performing spatial smoothing to an approach involving covariance matrix constructions, without really performing spatial smoothing. Again, note from [20] that although spatial smoothing solves the problem with coherent targets, it limits the performance in terms of identifiability of the number of sources, by making it worse than what an un-smoothed array works with non-coherent signals. Contrarily, the TF-based approach does not face such a bottleneck, yet achieves similar performance to that of spatial-smoothed results. This directly highlights the superiority of the work of this paper over conventional approaches. To study better about how well pairing of DOD-DOA is achieved with coherent targets, 'Detection Probability' is evaluated which gives an measure of how good the estimate can predict the actual, but an approximate DOA (up to an accuracy of $\pm 2^{\circ}$) of a target. It is given by,

$$\text{Detection Probability} = \frac{\text{Number of trials in which true DOA is detected}}{\text{Total number trials}}.$$

The detection probability plot is given in Figure 12(e) after averaging over 15 MC runs with SNR, separately for 2 targets along with the mean probability curve. Thus, even at considerably low SNRs, the achieved detection probability seems to be well within experimental requirements.

5. CONCLUSIONS AND FUTURE RESEARCH DIRECTIONS

In this paper, a more detailed attempt to integrate time-frequency analysis and direction finding algorithms has been made in the context of bistatic MIMO radars. Time Frequency based approach turns out to be a promising candidate for DOD-DOA estimation for bistatic MIMO radars, and specially it outperforms conventional approaches at lower SNRs. Furthermore, the TF based estimates attain the CRLB quickly at lower SNR regime. The TF based DOD-DOA estimates are consistent with very good resolution performance. On the other hand, it was also shown that TF integrated direction finding could potentially work better for a scenario with coherent targets, with enhanced performance with signals whose stationarity profile varies rapidly, which enhances the data independency. Some of the potential future research directions in this field include: 1) to recast the problem with coherent targets into one of a sparse recovery problem along with STFD construction, which can potentially render highly robust solutions with coherent targets, 2) to employ sparse arrays at transmitter/receiver with number of antennas less than that of targets and leverage TF representations. The intuition behind the latter point is to realize that at any given time instant, the instantaneous frequency laws are richly concentrated only for a subset of the total number of targets present. One other potential direction is to leverage the information from STFD matrices and build efficient adaptive algorithms (kalman filters) for tracking the targets, which are most prevalent in the discipline of radar signal processing.

REFERENCES

1. Skolnik, M. I., "An analysis of bistatic radar," *IRE Transactions on Aerospace and Navigational Electronics*, Vol. ANE-8, No. 1, 19–27, March 1961.
2. Chintagunta, S. and P. Ponnusamy, "Spatial and polarization angle estimation of mixed-targets in MIMO radar," *Progress In Electromagnetics Research M*, Vol. 82, 49–59, 2019.
3. Zhang, X., X. Gao, G. Feng, and D. Xu, "Blind joint DOA and DOD estimation and identifiability results for MIMO radar with different transmit/receive array manifolds," *Progress In Electromagnetics Research B*, Vol. 18, 101–119, 2009.
4. Foutz, J., A. Spanias, and M. K. Banavar, "Narrowband direction of arrival estimation for antenna arrays," *Synthesis Lectures on Antennas*, Vol. 8, 1–79, 2008.
5. Zheng, G. and B. Chen, "Unitary dual-resolution ESPRIT for joint DOD and DOA estimation in bistatic MIMO radar," *Multidimensional Systems and Signal Processing*, Vol. 26, No. 1, 159–178, 2013.
6. Chen, J., H. Gu, and W. Su, "A new method for joint DOD and DOA estimation in bistatic MIMO radar," *Signal Processing*, Vol. 90, No. 2, 714–718, 2010.
7. Xie, R., Z. Liu, and J. Wu, "Direction finding with automatic pairing for bistatic MIMO radar," *Signal Processing*, Vol. 92, No. 1, 198–203, 2012.
8. Ciuonzo, D., G. Romano, and R. Solimene, "Performance analysis of time-reversal MUSIC," *IEEE Transactions on Signal Processing*, Vol. 63, No. 10, 2650–2662, May 2015.
9. Devaney, A. J., "Time reversal imaging of obscured targets from multistatic data," *IEEE Transactions on Antennas and Propagation*, Vol. 53, No. 5, 1600–1610, May 2005.
10. Ciuonzo, D., "On Time-reversal imaging by statistical testing," *IEEE Signal Processing Letters*, Vol. 24, No. 7, 1024–1028, July 2017.
11. Li, J. and P. Stoica, *MIMO Radar Signal Processing*, 2008.
12. Khan, N. A., S. Ali, M. Mohammadi, and M. Haneef, "Direction of arrival estimation of sources with intersecting signature in time-requency domain using a combination of IF estimation and MUSIC algorithm," *Multidimensional Systems and Signal Processing*, 2019.
13. Zhang, Y., M. Amin, and B. Himed, "Joint DOD/DOA estimation in MIMO radar exploiting time-frequency signal representations," *EURASIP Journal on Advances in Signal Processing*, 2012.
14. Sergios T. and R. Chellappa, *Academic Press Library in Signal Processing, Volume 3: Array and Statistical Signal Processing*, 1st Edition, Chapter 3, Academic Press, Inc., USA, 2013.
15. Cohen, L., *Time-frequency Analysis: Theory and Applications*, Prentice-Hall, Inc., USA, 1995.

16. Amin, M. G. and Y. Zhang, "Spatial time-frequency distributions and their applications," *Proceedings of the Sixth International Symposium on Signal Processing and Its Applications*, 2001.
17. Amin, M. G. and Y. Zhang, "Direction finding based on spatial time-frequency distribution matrices," *Digital Signal Processing*, Vol. 10, No. 4, 325–339, 2000.
18. Stoica, P. and R. Moses, *Spectral Analysis of Signals*, Prentice Hall, Inc., Englewood Cliffs, NJ, USA, 2005.
19. Rao, B. D. and K. V. S Hari, "Analysis of subspace-based direction of arrival estimation methods," *Sadhana, Academic Proceedings in Engineering sciences*, Vol. 16, No. 3, 183–194, Nov. 1991.
20. Shan, T.-J., M. Wax, and T. Kailath,"On spatial smoothing for direction-of-arrival estimation of coherent signals," *IEEE Transactions on Acoustics, Speech, and Signal Processing*, Vol. 33, No. 4, 806–811, August 1985.
21. Subramaniam, K., P. Ponnusamy, and S. Chintagunta, "Polarization difference smoothing in bistatic MIMO radar," *Progress In Electromagnetics Research Letters*, Vol. 88, 67–74, 2020.
22. Lee, Y., C. Park, T. Kim, Y. Choi, K. Kim, D. Kim, M.-S. Lee, and D. Lee, "Source enumeration approaches using eigenvalue gaps and machine learning based threshold for direction-of-arrival estimation," *Applied Sciences*, Vol. 11, No. 1942, 2021.
23. Valaee, S. and P. Kabal, "An information theoretic approach to source enumeration in array signal processing," *IEEE Transactions on Signal Processing*, Vol. 52, No. 5, 1171–1178, May 2004.